TECHNISCHE MECHANIK
an open access journal

journal homepage: www.ovgu.de/techmech

Tech. Mech., Vol. 43, Is. 1, (2023), 151–161

Received: 27.01.2023
Accepted: 08.02.2023
Available online: 16.02.2023

Addressing wind comfort in an urban area using an immersed boundary framework

Patricia Vanky[1]*, Andreas Mark[2], Franziska Hunger [2], Marie Haeger-Eugensson[3], Joaquim Tarraso[4], Marco Adelfio[4], Angela Sasic Kalagasidis[4], and Gaetano Sardina[1]

[1] Chalmers University of Technology, Department of Mechanics and Maritime Sciences, Hörsalsvägen 7A, 412 96 Gothenburg, Sweden.
[2] Fraunhofer-Chalmers Research Centre for Industrial Mathematics, Sven Hultins gata 9, 412 58 Gothenburg, Sweden
[3] COWI AB, Section of Environmental Modelling and Sustainability Anlysis, Vikingsgatan 3, 411 04 Gothenburg, Sweden
[4] Chalmers University of Technology, Department of Architecture and Civil Engineering, Chalmersplatsen 4, 412 96 Gothenburg, Sweden

Abstract: Considering wind, air and heat comfort in designing new urban areas is still a challenge for city planners. Urban heat islands, or the phenomena of locally increased temperatures in urban areas compared to their rural surroundings, are becoming increasingly problematic with global warming and the rise of urbanization. Therefore, new areas must be planned considering appropriate ventilation to mitigate these high-temperature regions and cooling strategies, such as green infrastructures, must be considered. Typically, most of the comfort criteria are evaluated and assessed in the final stages of urban planning when further strategic interventions are no longer possible. Here, a numerical framework is tested that urban planners can use as a future tool to analyze complex fluid dynamics and heat transfer in the early stages of urban planning. The framework solves the RANS equations using an immersed boundary approach to discretize the complex urban topography in a cartesian octree grid. The grid is automatically generated, eliminating the complex pre-processing of urban topographies and making the framework accessible to all users. The results are validated against experimental data from wind tunnel measurements of wind-driven ventilation in street canyons. After validation, we will apply the numerical framework to estimate the wind comfort in an idealized urban area. Finally, guidelines will be provided on the choice of minimum grid sizes required to capture the relevant flow structures inside a canyon accurately.

Keywords: Immersed Boundary, Street Canyons, Urban climate, Ventilation

1 Introduction

Pedestrian wind comfort and wind safety are essential when planning urban areas, where narrow streets and high-rise buildings can accelerate the flow, creating uncomfortable and possibly unsafe regions. The comfort level in urban spaces determines their usage by urban citizens and visitors (Nikolopoulou et al., 2001), leaving shops in streets with high-velocities unattended and out of business (Wise, 1970). However, limiting the wind can also cause issues, such as ventilation of street canyons, an important factor in heat and air pollution mitigation. This makes for a complicated interaction to balance and requires close evaluation for optimization.

In addition, the local temperatures in urban areas are already higher than in their rural surroundings due to the built structure. This temperature difference is often referred to as Urban Heat Islands (UHI), and it can be tied to significant physical and mental health issues for residents and visitors of the cities (Huang et al., 2020). During summer, when the temperatures are already high, the UHIs increase mortality significantly, especially during heat waves (Smargiassi et al., 2009; Rydin et al., 2012). Nowadays, the World Health Organisation (WHO) classes heat waves as one of the most dangerous natural disasters, with 70,000 dead during the 2003 heat wave in Europe (McGregor et al., 2015). Furthermore, the Urban Heat Islands also both impact and are impacted by global warming, creating a spiraling effect of heated cities. As the temperature increases in the cities, the usage of energy-consuming equipment, such as air conditioning, rises (Hassid et al., 2000), contributing to global warming and, as a consequence, increasing the temperatures in the cities even further. With global urbanization, the number of people living in the cities has surpassed the majority in the last decade, and it is estimated that close to 70% of the world's population will be residing in urban areas by the year 2050 (United Nations, Department of Economic and Social Affairs, Population Division, 2018). Given that the majority of people will continue to be negatively affected by the increasing temperatures, it is essential to consider urban heat islands when planning and designing cities so that temperature mitigation is possible.

Several studies have been done on what attributes in urban design can improve urban comfort and limit the effect the UHIs (Pramanik and Punia, 2020; Ramírez-Aguilar and Souza, 2019; Vos et al., 2013; Alchapar et al., 2014). Key factors presented in these studies are land use, city density, the presence of urban blue and green spaces and thermal storage in building materials. In particular, the first two key factors are considered to increase heat mitigation by enhancing ventilation, while the others aim to limit heat storage by introducing cooling materials and natural blue and green areas. However, these design strategies are strongly interconnected; therefore, addressing their effects one by one as a possible solution without considering their interactions

* E-mail address: patricia.vanky@chalmers.se
doi: 10.24352/UB.OVGU-2023-052
2023 | All rights reserved.

is too simplistic. On the other hand, the coupling between heat storage, ventilation, and cooling strategies generates a complex system where the global effect of temperature mitigation is hard to predict. Therefore, modern urban design procedures have to be evaluated on their success in improving the thermal climate in practice. Typically, urban comfort is assessed in the final stages of urban planning when further strategic interventions are no longer possible due to the complexity of the assessment. For this reason, it is necessary to develop new and accurate numerical methodologies to assess the complex relations between fluid dynamics and heat transfer processes in urban regions so that urban designers can use them in the early stages of the design process.

Previous computational fluid dynamics (CFD) studies typically consider only one of the factors determining the urban environmental quality, either the wind (He and Song, 1999; Tominaga et al., 2008; Blocken et al., 2012; Antoniou et al., 2017) or the heat (Takahashi et al., 2004; Ashie and Kono, 2011; Wang et al., 2016). More recent studies (Antoniou et al., 2019; Brozovsky et al., 2021) show that the interest in these more complex combinations of wind and heat phenomena is increasing. However, CFD numerical simulations are still highly dependent on skilled professionals to generate the complex unstructured mesh needed to simulate all these phenomena.

This paper describes the validation of a user-friendly fluid dynamic numerical solver developed for predicting wind speed and ventilation in urban areas. The framework is based on an immersed boundary methodology which employs an automatically generated Cartesian octree grid, eliminating the complex pre-processing of urban topographies and making the framework accessible for general users with different backgrounds. The numerical tool is validated against wind tunnel experiments from Allegrini (2018) related to a typical urban topography area. Finally, we evaluate the wind comfort of an idealized urban neighborhood using the validated numerical framework.

2 Methodology

In this paper, the isothermal ventilation of urban street canyons is studied and validated against wind tunnel experiments.Turbulence is modelled using the one-equation model of Spalart-Allmaras for the turbulent viscosity.

2.1 Flow solver

The inputs to a wind simulation are an xml-file describing the simulation setup and a number of geometry files. In the setup xml-file the simulation domain, inlet conditions, grid refinements, residuals and turbulence model are defined. The input geometries consist of an oriented triangulated surface mesh that is automatically connected to the background grid describing the local topography of the terrain and the buildings.

Here, we use the steady-state version of the in-house flow solver, IBOFlow® (Mark et al., 2011) developed at Fraunhofer-Chalmers Research Centre. The solver integrates the Reynolds' averaged Navier-Stokes equations,

$$\nabla \cdot \vec{u} = 0, \tag{1}$$

$$\frac{\partial \vec{u}}{\partial t} + \vec{u} \cdot \nabla \vec{u} = -\frac{\nabla p}{\rho} + \nabla \cdot ((\nu + \nu_t)\nabla \vec{u}), \tag{2}$$

along with the turbulent transport equations. In the above equations, $\vec{u}$ is the mean velocity field, ρ the air density, p the mean pressure, ν and ν_t are the molecular and turbulent kinematic viscosities. The finite volume method discretises all equations on a Cartesian octree grid that is automatically refined around the geometries. The Navier-Stokes equations are solved in a segregated manner, and the SIMPLEC method derived in Van Doormaal and Raithby (1984) is used to couple the pressure and the velocity fields. All variables are stored in a co-located arrangement, and the pressure-weighted flux interpolation proposed in Rhie and Chow (1983) is used to suppress pressure oscillations. The steady-state solver is based on artificial time stepping and solved until all relative solution residuals are lower than the specified residual. Finally, the mirroring immersed boundary method (Mark and van Wachem, 2008) is employed to model the presence of all geometries without needing a body-fitted mesh.

In this paper the turbulence model Spalart-Allmaras is used for all calculations. The Spalart-Allmaras model evolves the kinematic turbulent eddy viscosity that is given by $\nu_t = f_{v1}\tilde{\nu}$, where the viscous damping is given by $f_{vt} = \frac{\chi^3}{\chi^3 + c_{v1}^3}$, and $\chi = \frac{\tilde{\nu}}{\nu}$. $\tilde{\nu}$ is given by

$$\frac{\partial \tilde{\nu}}{\partial t} + \vec{u} \cdot \nabla \tilde{\nu} = P - D + \frac{1}{\sigma}\left[\nabla \cdot ((\nu + \tilde{\nu})\nabla \tilde{\nu}) + c_{b2}|\nabla \tilde{\nu}|^2\right] \tag{3}$$

where P is the production term and D is the destruction term. For complete description see Allmaras et al. (2012). $\tilde{\nu}$ is set to zero on the geometries with help of the implicit immersed boundary condition.

2.2 Experimental and Simulation Set Up

The aim is to validate the solver using the Particle Image Velocimetry (PIV) experimental data by Allegrini (2018), where a compilation of blocks of various sizes are placed in a wind tunnel to describe a prototypal urban area. The test domain consists of a 5x5 row configuration of buildings with straight, continuous streets between them forming regular canyons. In front of these buildings, a set of irregularly sized shaped and placed buildings is inserted to create an irregular flow pattern representing that of a typical city. The flat roof height, H, of these buildings is equal to 14 cm. In one of the street canyons between the organized

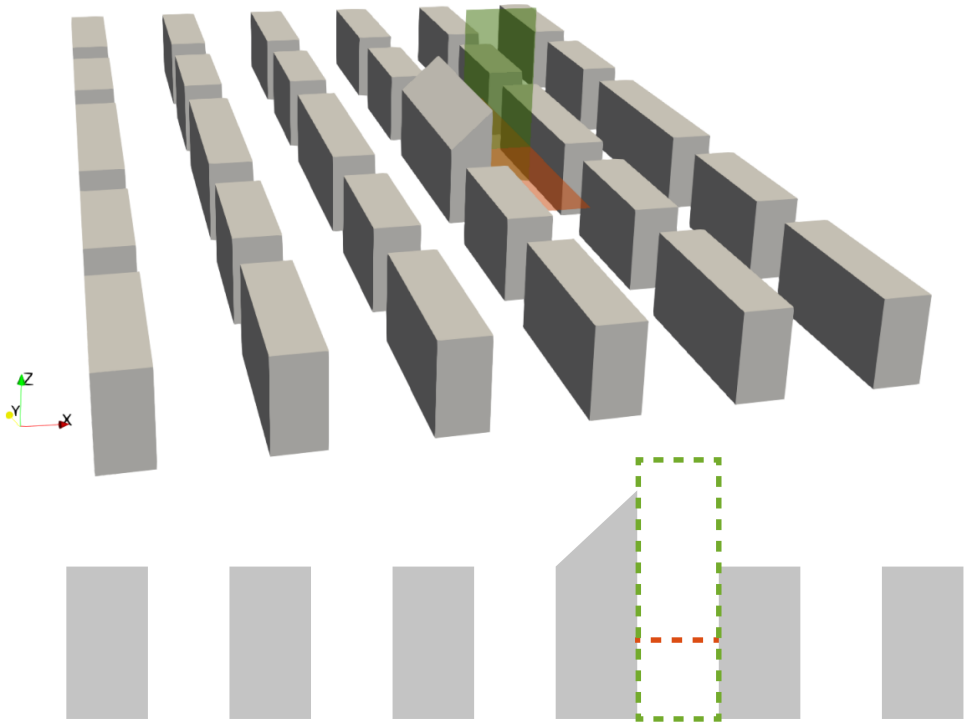

Fig. 1: Top: 3D visualization of the domain where the red and green planes show the horizontal and vertical PIV-planes, respectively. Bottom: 2D side view, PIV-planes showed as dashed lines in green and red.

buildings, the air velocity is measured using PIV. Some modifications are made to this setup to create five different cases to study the flow field, namely case A-E. Case A is the case just described, while the other cases consist in changing the inclination of the roof of the leading building (cases B and C) or changing the width of the leading and trailing (cases D and E) building in the measured canyon.

Here, the case called Case C in Allegrini (2018) will be analyzed for an inlet velocity, U_{ref}, of 1.94 m/s at the height of $2H$ with a profile formulated as by Richards and Hoxey (1993). This case was chosen as it includes a building with a pitched roof leading up to the measured street canyon, adding domain complexity to the otherwise flat roofs and inducing a separation region inside the canyon. The wind tunnel data correspond to a vertical and horizontal velocity plane from Particle Image Velocimetry (PIV) measurements, shown in Fig.1. The vertical plane is located at the center of the canyon, and the horizontal plane is set at half of the flat roof height. A complete simulation of the entire wind tunnel chamber is too computationally expensive; therefore, the simulations were performed over a portion of the domain consisting of six lines of buildings. In addition, a flat region was added at the beginning to develop the flow instead of the irregular buildings in the experiment. Several preliminary tests on the initial geometry and domain streamwise lengths have been performed to achieve a compromise between quality of the results and computational time. Fig.1 shows the final domain configuration with 6x5 rows of buildings that, together with the developing region, gives a domain of the size 2.0 x 1.9 x 0.85 m. The PIV-planes are marked in red (horizontal) and green (vertical) in the top panel and as dashed lines in the bottom panel.

The grid of the simulation domain is set up with a uniform base cell size of $0.05 \times 0.05 \times 0.05$ m, which is refined around the near-wall regions of the ground and buildings. The ground and buildings along the sides of the domain are refined two times, whereas the six buildings along the middle column, where the PIV-planes are located, are refined further, up to four additional refinements corresponding to 48 grid points inside the canyon and a total of approximately five million cells in the domain. A grid study to find the number of refinements to reach numerical convergence of the mean velocity field will be described in the Results section.

The conditions of the wind tunnel experiment represents a Reynolds number, $Re = U_{ref} L_c / \nu$, of approximately 17000, using a characteristic length, L_c, equal to the building height, H, and air properties at a temperature of 20 °C. This Reynolds number is around an order of magnitude lower than what it usually is within a city, although above the critical Reynolds number, $Re_c = 11000$, for Reynolds number independence in street canyons with aspect ratio, $H/W = 1$ (Chew et al., 2018). In case C, however, the building at the leading edge of the canyon is taller, and the aspect ratio can not be easily defined due to the height variation. A complementing simulation to the experimental conditioned case is therefore run with a simulation using an inlet velocity of an order of magnitude higher, $U_{ref} = 19.4$ m/s, also increasing the Reynolds number by an order to evaluate whether Reynolds number independence has been reached.

The last step of the numerical validation consists of a convergence study performed by monitoring the order of magnitude of the

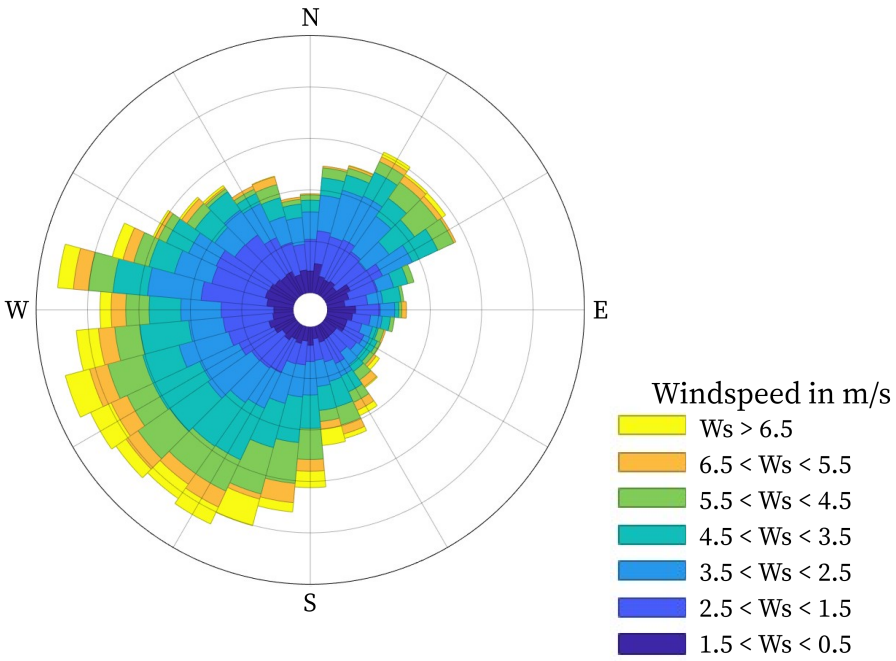

Fig. 2: Windrose from hourly data measured during a year at a wind station in Gothenburg, Sweden.

residuals needed to reach a steady solution.

2.3 Annual Average Wind

The wind direction and speed in both rural and urban areas changes with the seasonal variations of the weather, it can therefore be of interest to observe the wind conditions in urban regions as annual averages. In urban areas, there are often wind stations measuring hourly data of wind direction and wind speed that can be summarized into annual average (SMHI, 2022); in combination with CFD, these wind conditions can be presented as annual average wind fields. Simulations done on the annual average in cities are usually run for one wind velocity and several wind directions (Willemsen and Wisse, 2002). The velocities are then scaled to the range of measured wind velocities and create a set of occurring wind conditions, assuming that Reynolds number independence is satisfied. These results are then combined into an annual average by summing all simulated wind conditions multiplied by the frequency of their occurrence over the year.

The frequencies for the occurrence of wind conditions for these simulations are based on measurements from a wind station at the height of 10 m located in Gothenburg, Sweden, where the distribution can be seen in Figure 2. The measurements show that the predominant wind direction in the region is west/southwest. Therefore, the simulated results can be rotated to vary which domain face is aligned with the north direction of the measured frequencies and, thereby, the predominant wind direction. The annual average results from the differently orientated cities can then be used to evaluate the most favorable orientation in terms of street canyon ventilation in the preliminary planning phases of new urban areas.

To generate an annual averaged velocity field within the street canyon in this wind tunnel case, the domain was then simulated in eight directions with a 45 °interval. The idealized city was modified so that the street canyon of interest was placed in the middle, with three rows of buildings both up- and downstream. Each simulation domain is manipulated to ensure an equally long developing region upstream of the idealized city for all simulation directions. For the simulations, an inlet velocity of U_{ref} = 5 m/s at the height of $2H$ was used with the same profile as previous simulations. The velocities are then scaled to 0.5, 1.5, 2.5, 3.5, 4.5, 5.5 and 6.5 m/s at the height of 10 cm to generate all wind conditions found in the measured data used for averaging assuming Reynolds independence of the mean velocity field. This assumes the scale of the domain to be 1:100, representing buildings of height 14 m.

3 Results

Comparisons between the wind tunnel data and the numerical simulations can be made by observing the velocity contours over the PIV-planes and the one-dimensional (1D) velocity over the center line of the previously defined planes.

3.1 Grid Study

A grid optimization study has been performed to accurately evaluate the minimum number of cells to solve the mean flow field inside the canyon. The case under investigation, using the Spalart-Allmaras model and a value of maximum relative residual of

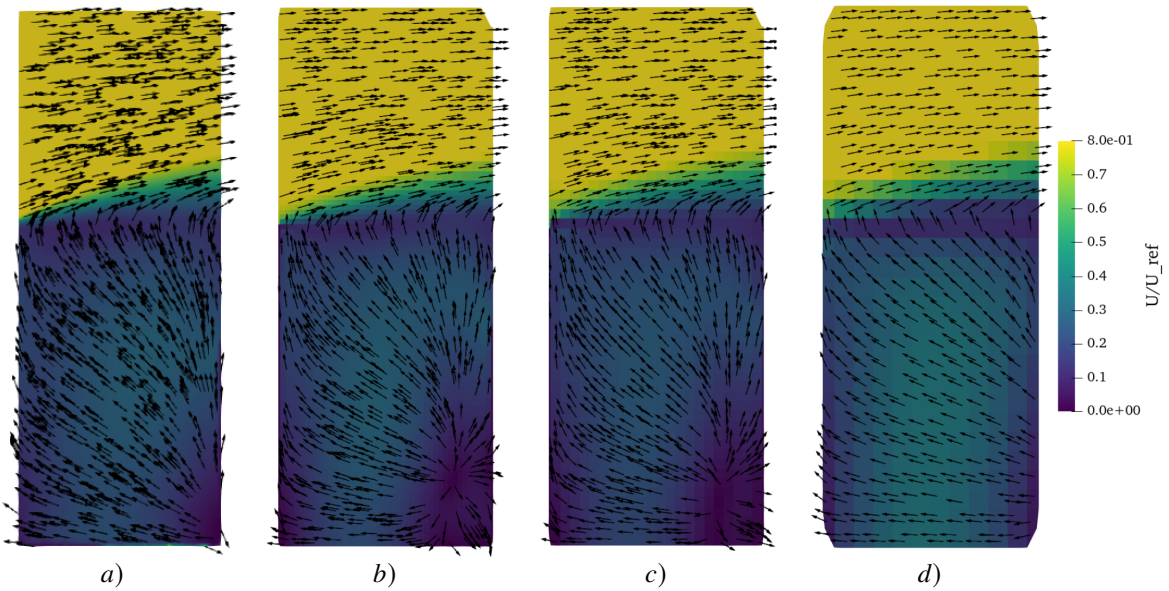

Fig. 3: Contour plots and streamlines of the in-plane mean velocity magnitude on the vertical plane. The panels represent the PIV data (a) followed by the results of three simulations with different grid resolutions, b) 4 refinements, c) 3 refinements, and d) 2 refinements

10^{-6}, has been run using three different grids. The three grids employ two, three and four refinements in the cells surrounding the measured canyon, corresponding to 12, 24 and 48 cells along the canyon width. The results are presented in Figures 3 and 4.

Fig.3 shows the contours of the in-plane mean velocity magnitude on the vertical plane for the experimental (a) and the numerical data (b-d) at different resolutions. Comparing the different results, we obtain a fair agreement against the experimental data for the four and three refinements grid as a qualitative impression. On the other hand, the simulation in the most coarse grid shows a large part of the canyon with low-velocity magnitude probably induced by numerical dissipation. Moreover, the experimental data show a recirculation region in the lower right corner of the canyon, a feature captured by both the most refined simulations but not by the two refinement mesh. This would indicate that some important fluid dynamics phenomena might be missed if the mesh is not refined well enough.

To have a quantitative comparison between the different solution fields, we plot in Fig. 4 the vertical (left panel) and horizontal (right panel) profile of the horizontal mean velocity component. Both profiles confirm the qualitative impression obtained by the previous figure that grid convergence is reached by the two most resolved grids using four and three refinements. The coarser grid predicts a lower mean velocity inside the canyon close to the ground to then become similar after the roof level. The bottom panel shows that the velocity in the coarser grid differs at the center of the perpendicular street canyon, with a fair agreement to the experimental velocity close to the street canyons parallel to the wind. To conclude, the grid study shows that 24 cells per canyon are sufficient. A coarser mesh can give fair results overall, but fails to predict detailed results of the flow field inside the canyon.

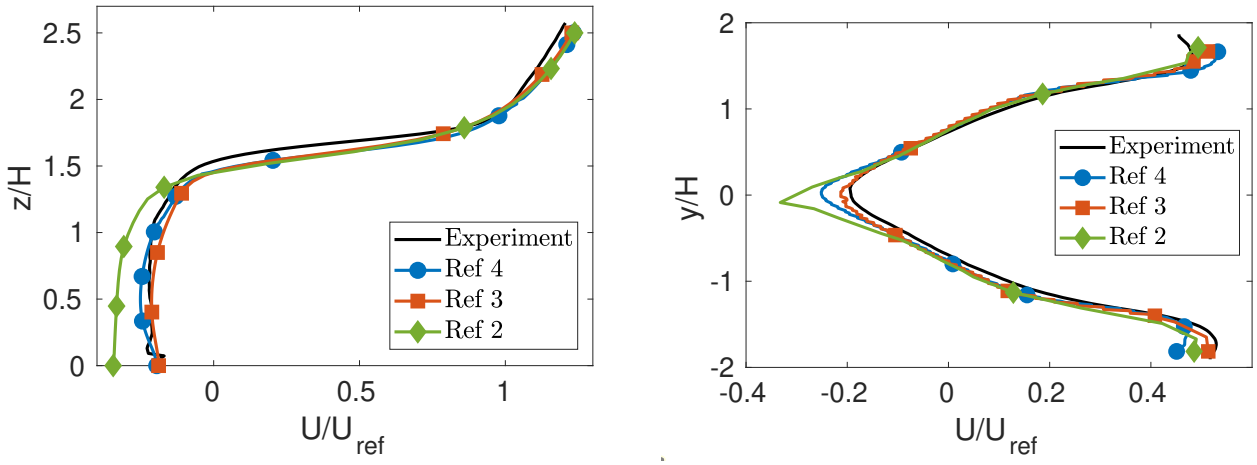

Fig. 4: Vertical (left panel) and horizontal profiles (right panel) of the horizontal average velocity component at the center of the street canyon for case C. The simulation results with grid refinements (solid lines with symbols) are compared against PIV experimental data (solid black line).

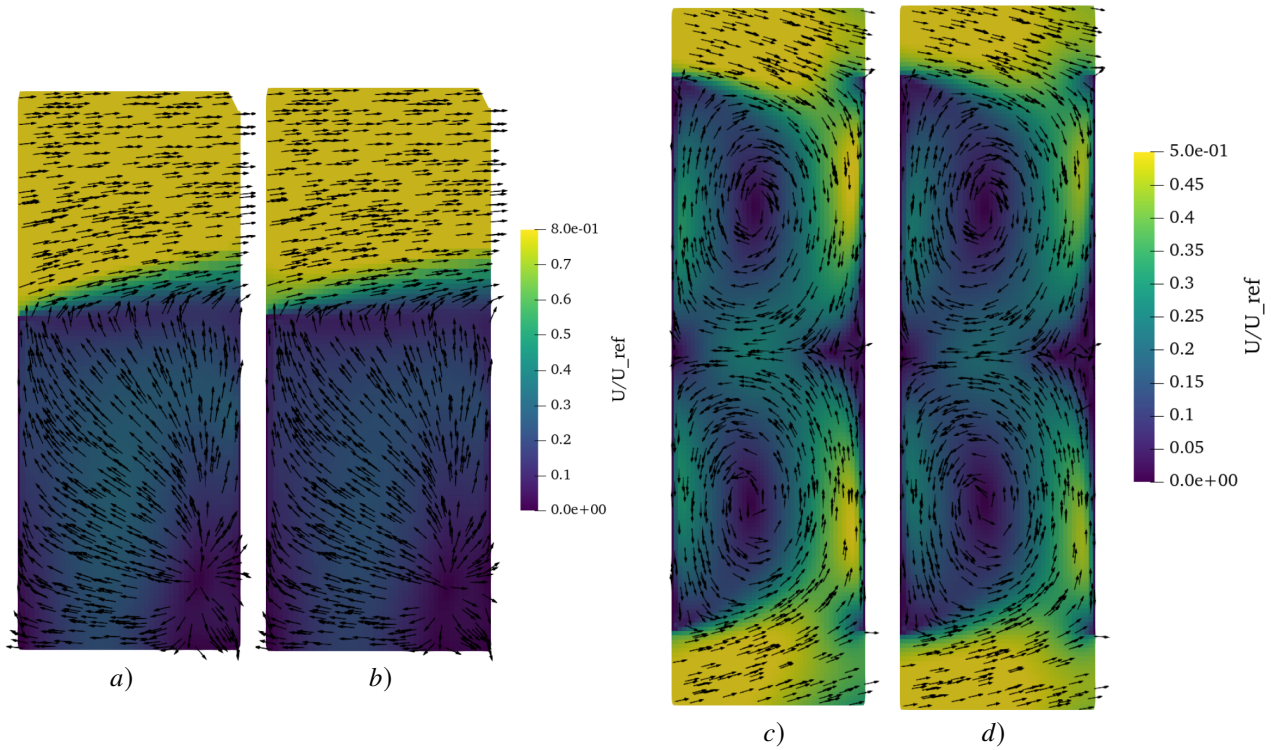

Fig. 5: Contour plots and streamlines of the in-plane mean velocity magnitude for a variation of Reynolds number. (a) Re = 17 000 on the vertical plane, (b) Re = 170 000 on the vertical plane. (c) Re = 17 000 on the horizontal plane, (d) Re = 170 000 on the horizontal plane.

3.2 Reynolds Number Independence

In practice, we want to avoid running different simulation configurations corresponding to different wind velocities and directions that occur during a period of one year. If the flow field is Reynolds independent, the normalized velocities rescaled with the inlet velocity are self-similar, so it is sufficient to run just one case for each wind direction. In order to test this property, we run an additional case with a Reynolds number (170000) that is ten times the one achieved in the wind tunnel. Moreover, this Reynolds number value is typical of a more realistic urban environment. A comparison of the non-dimensional velocity distribution, normalized by the reference velocity, in Fig.5, shows a self-similar profile for both Reynolds numbers for the normalized velocities. This would mean that Reynolds number independence has been achieved even if the aspect ratio criterium was not fulfilled and that the lower Reynolds number used in the experiments will yield flow patterns that can be expected at an urban scale. Further, it means that scaling the wind velocities when generating all wind conditions for an annual average can also be safely applied since changing the Reynolds number would not affect the characteristics of the wind field.

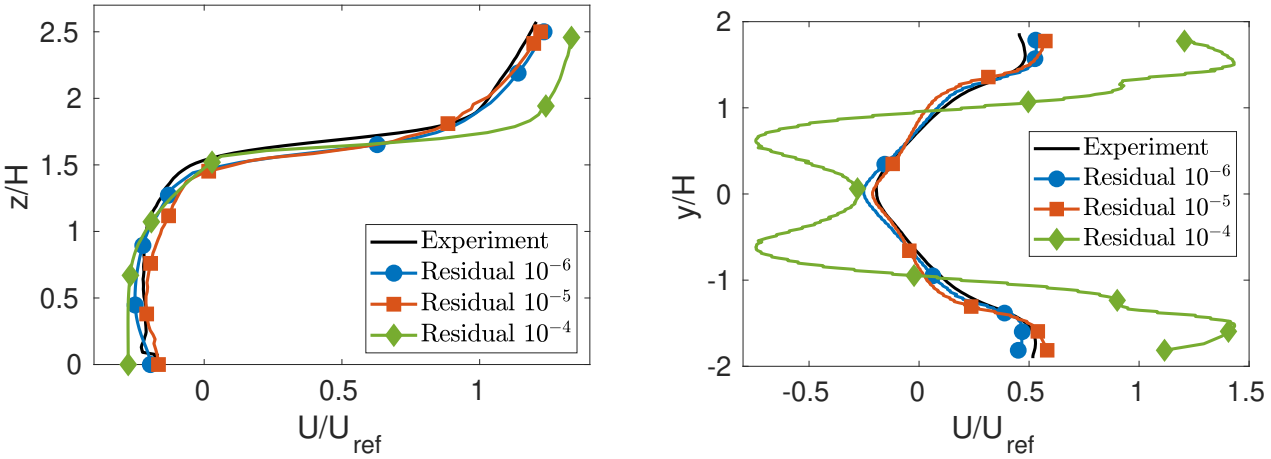

Fig. 6: Convergence towards the steady-state of vertical 1D velocity for the case C of the experiments over the vertical and horizontal PIV plane respectively. Residual 10^{-4}, 10^{-5} and 10^{-6} compared to experimental velocity

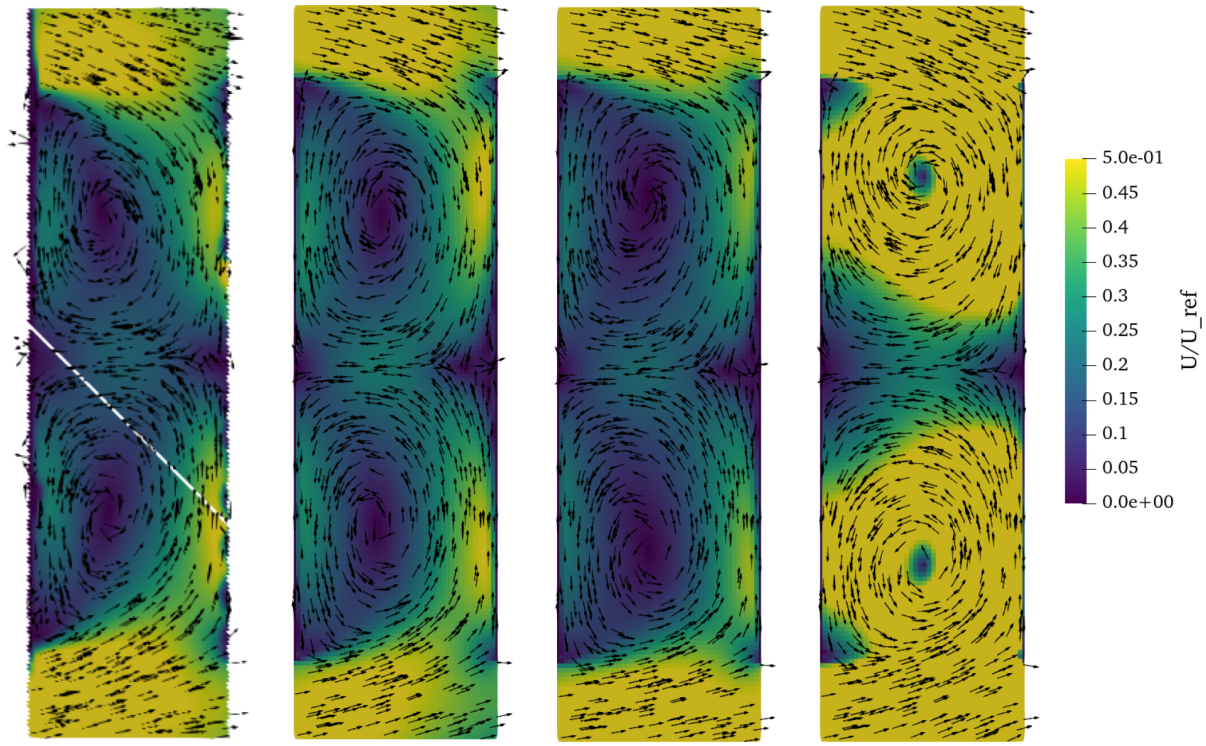

Fig. 7: Contour plots and streamlines of the in-plane average velocity magnitude on the horizontal plane for different residuals: a) Reference experimental results, b) residual 10^{-6}, c) residual 10^{-5}, d) residual 10^{-4}.

3.3 Residuals

The convergence towards the steady-state solution has been evaluated by comparing the numerical horizontal mean velocity profiles with maximum residuals of 10^{-4}, 10^{-5} and 10^{-6} to the experimental velocities in Figures 6 and 7. With both residuals of 10^{-6} and 10^{-5}, the simulated results are good in the entire canyon region and can be considered converged.

The reasons for the mismatches can be seen in Fig. 7 for a residual of 10^{-4}; the recirculation regions in the horizontal velocity plane have started to form but are not yet fully developed. This explains the high velocities that are found in the bottom panel of Fig. 6 and also the large negative velocities around the canyon center that are not seen in the most resolved cases. The flow simply needs additional iterations before it can be fully developed; therefore, the lower residual is insufficient. The contours also show that, although the 1D velocities show slight variation between residual 10^{-5} and 10^{-6}, the flow does develop slightly to come even closer to the experimental results for the finest convergence. However, a residual of 10^{-5} can indeed be considered sufficiently converged in cases where high computational time is an issue.

3.4 Annual Average Velocity Field and Wind Comfort

The results of the annual average velocity field will, of course, depend on what has been chosen as the northern direction of the idealized city since the predominant wind direction will vary. In this case, the results will be shown for two different orientations: a case where the north is aligned with the original experimental setup's inlet condition and the opposite direction, where the original inlet direction is aligned with the south. As mentioned, the predominant wind direction of the measured region is the south/southwest direction, which means that there will be less impact from the leading pitched roof building for the first case seen in the validation previously than if the predominant direction had been aligned with the experimental setup direction as in the second case.

The annual average velocity directions for the two different domain rotations can be seen in Fig.8. In both cases, the wind directions properly align with expectations based on the predominating wind conditions shown in Fig.2. The horizontal plane velocity fields (c and d) both show that the dominant western flow limits the vortices previously seen when the flow was perpendicular to the canyon. Therefore, we observe a crossflow velocity through the canyon that increases urban ventilation and could improve air quality and heat mitigation; however, it might also increase the velocity magnitudes, affecting wind comfort. The variation of wind comfort would need further investigation as the velocity magnitudes have not been evaluated. The vertical planes (a-b) also show better ventilation as the flow seems to exit the canyon at roof height for both rotations, even if the domain where north is aligned with the inlet direction (a) introduces a larger central vortex in the canyon and the opposite direction has the recirculation in the corner as seen in the previous validation.

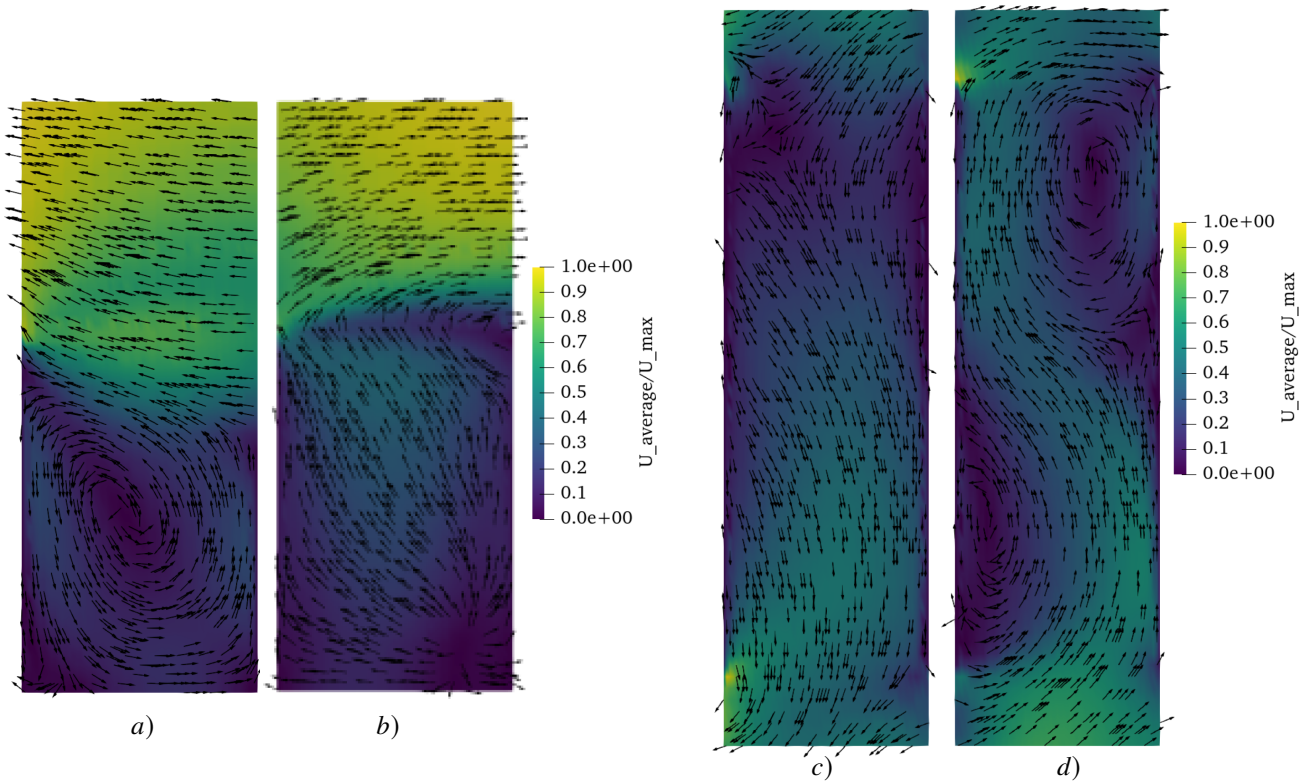

Fig. 8: Streamlines of the in-plane average velocity direction and contours of velocity magnitude normalized by the maximum velocity for two domain rotations. a) Vertical velocity field with north aligned with the inlet, b) vertical velocity field with south aligned with the inlet, c) horizontal velocity field with north aligned with the inlet, d) horizontal velocity field with south aligned with the inlet.

As mentioned, the average velocity fields can provide indications regarding the ventilation of the street canyon but do not address the comfort level for pedestrians in the area. Wind comfort in urban regions has been defined in literature by several different criteria, some of the most referenced one being the Davenport (Davenport and Isyumov, 1975), multiple versions of the Lawson (Lawson and Penwarden, 1975; Lawson, 1978, 1990) and the Dutch wind nuisance standard (NEN, 2006). Here, we use the original Lawson wind comfort criterion introduced in 1975, which categorizes wind comfort into five levels based on the wind velocity and accepted activities when the probability of the specific velocities occurring is less than 2%. The activities and the velocity ranges are listed in Table 1. The first category allows for activities such as sitting for long periods of time when the probability of velocities surpassing 1.8 m/s is less than 2%, while slowly strolling is considered comfortable in regions where the velocity does not exceed 5.3 m/s more than 2% of the time. The last category is labeled as uncomfortable regardless of activity and occurs when the probability of velocities over 7.6 m/s exceeds 2%. These comfort levels could be used when planning cities. For example, in regions where the comfort level suggests sitting for short periods of time, it could be appropriate to place benches to rest at, but it would be wise to avoid outdoor dining.

Tab. 1: Lawson comfort criterion categories

Category	Velocity	Probability	Activity
1	> 1.8m/s	$< 2\%$	Sitting long
2	> 3.6m/s	$< 2\%$	Sitting short
3	> 5.3m/s	$< 2\%$	Slow stroll
4	> 7.6m/s	$< 2\%$	Walking fast
5	> 7.6m/s	$\geq 2\%$	Uncomfortable

The fulfillment of the Lawson comfort criterion has been evaluated over a horizontal plane at pedestrian height (1.5 m above ground at the urban scale, 1.5 cm in the scaled model) in the simulated idealized city domain and can be seen in Fig. 9 for the two domain rotations. The same setup was used when the annual average velocity field was simulated, and the probability of occurrence was based on the frequency in the measured wind conditions. To apply this in practice, we first determined the probability of each inlet wind condition occurring based on how frequently it appeared in the measured hourly data. Then, the velocities in each cell were checked against the comfort criterion to see if they exceeded the threshold. If they did, the probability of the corresponding inlet condition was added to that cell. Finally, once the velocities in all cells and for all simulation directions had been checked, the total summation of the probabilities of a velocity condition occurring in each cell was used to determine the most appropriate comfort criterion category for that cell.

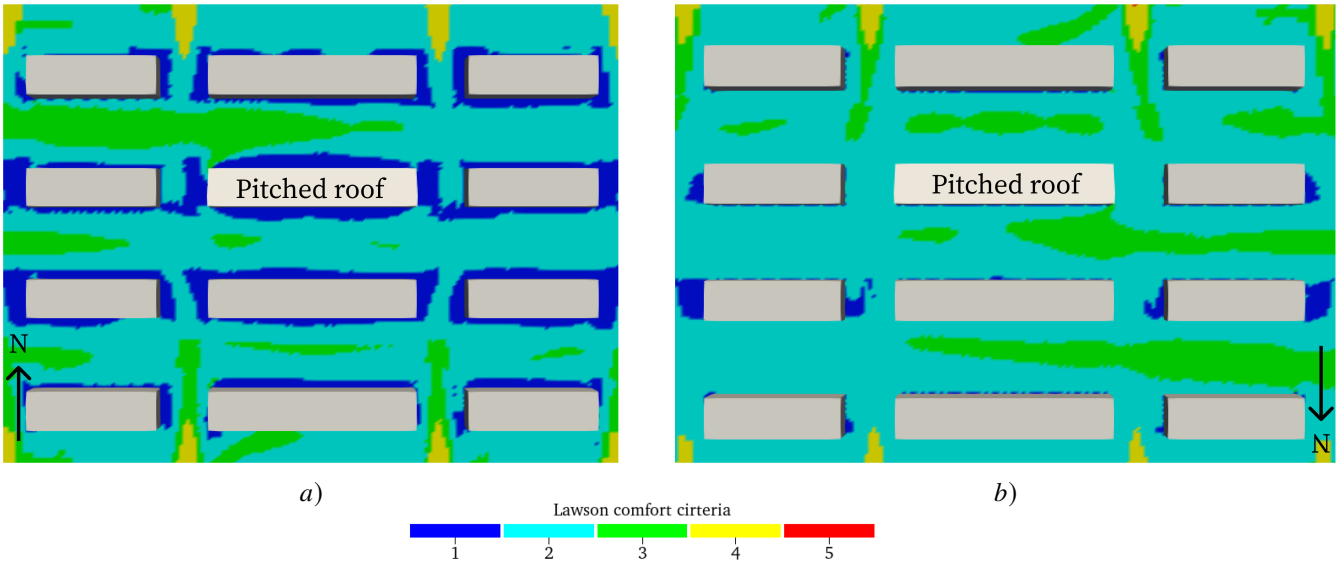

Fig. 9: Evaluation of the Lawson wind comfort criteria over the simulated domain at a pedestrian level based on wind velocities and frequency of measured data. a): the north direction aligned with the inlet of the original experimental setup. b): the south direction aligned with the inlet of the original experimental setup.

The results show that no uncomfortable areas are present in the domain and that most of the area is comfortable for sitting. This is not surprising as the domain is idealized with low height-to-width aspect ratios and no narrow streets where the Venturi effect accelerates the flow. The higher velocity regions are limited mainly to the inlet region of the predominant wind directions, as the buildings have not yet decelerated the flow there. An interesting note is also that even though the city is fully symmetrical for the two domain rotations except for the location and orientation of the pitched roof building, the variation in comfort levels between the two domains is quite noticeable. The flow is accelerated in all street canyons surrounding the pitched roof building for the right panel, significantly limiting the amount of comfort level 1 area. It would be interesting to evaluate the flow for a domain with more variations in building heights to see the flow development for more complex cases. In any case, it is clear that the flow pattern becomes increasingly more unpredictable as complexity is introduced, making the evaluation of wind in city development still a challenge for urban planners when the building height, street width and several other factors are considered.

4 Conclusion and outlook

A series of simulations have been conducted to validate a numerical framework against wind tunnel experiments of wind behavior and ventilation in urban street canyons with good agreement. It was found that the center of the street canyon is where it is hardest to estimate the wind velocity. However, it is possible to reach sufficient accuracy with high enough resolution. The necessary resolution has been estimated to be approximately 24 cells inside the canyon. Note that this resolution in the canyons has been evaluated for a small-scale test in a wind tunnel. Using 24 cells per canyon in a full-scale model, where a narrow street might be approximately 6-8 meters wide, implies a cell size of fewer than 0.5 meters which might not be feasible for domains of several square kilometers. This computational aspect will be further investigated in future works. In addition to necessary grid resolution, it has been found that a residual of at least 10^{-5} is needed to reach a steady-state converged solution. It has also been established that Reynolds number independence is reached for the domain configuration, meaning that the low Reynolds number experiment gives an accurate representation of an urban scale velocity field.

The experimental domain was used to calculate the annual average velocity field in two different city orientations. It was found that, as expected, aligning the street canyon with the predominant wind direction increases the ventilation. Through evaluation of the wind comfort in the domain, it was also found that the taller pitched roof building forces the flow into alternative routes than if the building structure was fully symmetrical. This shows that wind assessment and comfort evaluation are crucial for planning functional and safe cities.

In this paper, we have only considered the wind behavior in an isothermal urban area. However, in Allegrini (2018), the same test cases have also been performed considering the impact of heat transfer. Our future developments will focus on implementing and investigating buoyancy effects due to the introduced heat in the wind tunnel cases. Moreover, we plan to introduce heat storage in building materials for façades and the ground, radiative heat transfer, and latent heat effects due to vegetation or blue areas. The final solver will constitute a complete tool for realistic urban area simulations that can be employed and easily used by urban planners to design and develop future sustainable cities.

Acknowledgements

This work was supported by the Swedish Research Council for Sustainable Development Formas under the grants 2019-01169 and 2019-01885. The computations were enabled by resources provided by the Swedish National Infrastructure for Computing (SNIC) at HPC2N partially funded by the Swedish Research Council through grant agreement no. 2018-05973. This work is also part of the Digital Twin Cities Centre supported by Sweden's Innovation Agency Vinnova under Grant No. 2019-00041. Finally, we would like to thank Professor Jan Carmeliet and his team at ETH for allowing the usage of experimental data for simulation validation purposes in this paper.

References

N.L. Alchapar, E.N. Correa, and M.A. Cantón. Classification of building materials used in the urban envelopes according to their capacity for mitigation of the urban heat island in semiarid zones. *Energy and Buildings*, 69:22–32, 2014.

J. Allegrini. A wind tunnel study on three-dimensional buoyant flows in street canyons with different roof shapes and building lengths. *Building and Environment*, 143:71–88, 2018.

S.R. Allmaras, F.T. Johnson, and P.R. Spalart. Modifications and non-linear in the boundary layer. several validation cases clarifications for the implementation of the Spalart-Allmaras in both two and three dimensions were provided, exhibit- turbulence model. *Seventh International Conference on Computational Fluid Dynamics (ICCFD7)*, 2012.

N. Antoniou, H. Montazeri, H. Wigo, M.K.A. Neophytou, B. Blocken, and M. Sandberg. CFD and wind-tunnel analysis of outdoor ventilation in a real compact heterogeneous urban area: Evaluation using "air delay". *Building and Environment*, 126:355–372, 2017.

N. Antoniou, H. Montazeri, M. Neophytou, and B. Blocken. CFD simulation of urban microclimate: Validation using high-resolution field measurements. *Science of the Total Environment*, 695:133743, 2019.

Y. Ashie and T. Kono. Urban-scale CFD analysis in support of a climate-sensitive design for the Tokyo bay area. *International Journal of Climatology*, 31(2):174–188, 2011.

B. Blocken, W.D. Janssen, and T. van Hooff. CFD simulation for pedestrian wind comfort and wind safety in urban areas: General decision framework and case study for the Eindhoven university campus. *Environmental Modelling Software*, 30:15–34, 2012. ISSN 1364-8152.

J. Brozovsky, A. Simonsen, and N. Gaitani. Validation of a CFD model for the evaluation of urban microclimate at high latitudes: A case study in trondheim, norway. *Building and Environment*, 205:108175, 2021.

L.W. Chew, A.A. Aliabadi, and L.K. Norford. Flows across high aspect ratio street canyons: Reynolds number independence revisited. *Environmental Fluid Mechanics*, 18(5):1275–1291, 2018.

A.G. Davenport and N. Isyumov. The ground level wind environment in built-up areas. In *Proceedings of Fourth International Conference on Wind Effects on Buildings and Structures*, pages 403–422. Cambridge University Press, September 1975.

S. Hassid, M.N.A.N.C. Santamouris, N. Papanikolaou, A. Linardi, N. Klitsikas, C. Georgakis, and D.N. Assimakopoulos. The effect of the athens heat island on air conditioning load. *Energy and Buildings*, 32(2):131–141, 2000.

J. He and C.C.S. Song. Evaluation of pedestrian winds in urban area by numerical approach. *Journal of Wind Engineering and Industrial Aerodynamics*, 81(1-3):295–309, 1999.

H. Huang, X. Deng, H. Yang, S. Li, et al. Spatial evolution of the effects of urban heat island on residents' health. *Tehnički vjesnik*, 27(5):1427–1435, 2020.

T.V. Lawson. The wind content of the built environment. *Journal of Wind Engineering and Industrial Aerodynamics*, 3(2-3): 93–105, 1978.

T.V. Lawson. The determination of the wind environment of a building complex before construction. *Department of Aerospace Engineering, University of Bristol, Report Number TVL*, 9025, 1990.

T.V. Lawson and A.D. Penwarden. The effects of wind on people in the vicinity of buildings. In *Proceedings of Fourth International Conference on Wind Effects on Buildings and Structures*, pages 605–622. Cambridge University Press, September 1975.

A. Mark and B.G.M. van Wachem. Derivation and validation of a novel implicit second-order accurate immersed boundary method. *Journal of Computational Physics*, 227(13):6660–6680, 2008.

A. Mark, R. Rundqvist, and F. Edelvik. Comparison between different immersed boundary conditions for simulation of complex fluid flows. *Fluid Dynamics & Materials Processing*, 7(3):241–258, 2011.

G.R. McGregor, P. Bessmoulin, K. Ebi, and B. Menne. *Heatwaves and health: guidance on warning-system development.* WMOP, 2015.

NEN. Wind comfort en wind danger in the built environment. Standard, NEN, The Netherlands, February 2006.

M. Nikolopoulou, N. Baker, and K. Steemers. Thermal comfort in outdoor urban spaces: understanding the human parameter. *Solar energy*, 70(3):227–235, 2001.

S. Pramanik and M. Punia. Land use/land cover change and surface urban heat island intensity: source–sink landscape-based study in Delhi, India. *Environment, Development and Sustainability*, 22(8):7331–7356, 2020.

E.A. Ramírez-Aguilar and L.C.L. Souza. Urban form and population density: Influences on urban heat island intensities in bogotá, colombia. *Urban Climate*, 29:100497, 2019.

C.M. Rhie and W.L. Chow. Numerical study of the turbulent flow past an airfoil with trailing edge separation. *AIAA Journal*, 21 (11):1525, 1983.

P.J. Richards and R.P Hoxey. Appropriate boundary conditions for computational wind engineering models using the k-ε turbulence model. *Journal of Wind Engineering and Industrial Aerodynamics*, 46:145–153, 1993.

Y. Rydin, A. Bleahu, M. Davies, J.D. Dávila, S. Friel, G. De Grandis, N. Groce, P.C. Hallal, I. Hamilton, P. Howden-Chapman, et al. Shaping cities for health: complexity and the planning of urban environments in the 21st century. *The Lancet*, 379(9831): 2079–2108, 2012.

A. Smargiassi, M.S. Goldberg, C. Plante, M. Fournier, Y. Baudouin, and T. Kosatsky. Variation of daily warm season mortality as a function of micro-urban heat islands. *Journal of Epidemiology & Community Health*, 63(8):659–664, 2009.

SMHI. Vind, 2022. URL https://www.smhi.se/data/meteorologi/vind.

K. Takahashi, H. Yoshida, Y. Tanaka, N. Aotake, and F. Wang. Measurement of thermal environment in Kyoto city and its prediction by CFD simulation. *Energy and Buildings*, 36(8):771–779, 2004. ISSN 0378-7788. Performance Simulation for Better Building Design.

Y. Tominaga, A. Mochida, R. Yoshie, H. Kataoka, T. Nozu, M. Yoshikawa, and T. Shirasawa. AIJ guidelines for practical applications of CFD to pedestrian wind environment around buildings. *Journal of Wind Engineering and Industrial Aerodynamics*, 96 (10-11):1749–1761, 2008.

United Nations, Department of Economic and Social Affairs, Population Division. World Urbanization Prospects: The 2018 Revision, 2018. Online Edition.

J.P. Van Doormaal and G.D. Raithby. Enhancements of the SIMPLE method for predicting incompressible fluid flows. *Numerical Heat Transfer*, 7(2):147, 1984.

P. E.J. Vos, B. Maiheu, J. Vankerkom, and S. Janssen. Improving local air quality in cities: to tree or not to tree? *Environmental Pollution*, 183:113–122, 2013.

Y. Wang, U. Berardi, and H. Akbari. Comparing the effects of urban heat island mitigation strategies for Toronto, Canada. *Energy and Buildings*, 114:2–19, 2016.

E. Willemsen and J.A. Wisse. Accuracy of assessment of wind speed in the built environment. *Journal of Wind Engineering and Industrial Aerodynamics*, 90(10):1183–1190, 2002.

A.F.E. Wise. *Wind effects due to groups of buildings*, volume 23. Building Research Station Garston, Watford, England, 1970.